A Self-Powered Photoelectrochemical Glucose Biosensor Based on Supercapacitor Co_3O_4-CNT Hybrid on TiO_2

Bekir Çakıroğlu, Mahmut Özacar

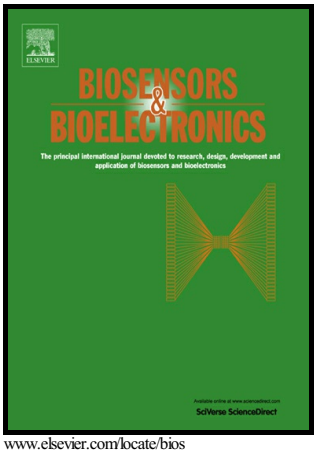

www.elsevier.com/locate/bios

PII: S0956-5663(18)30552-9
DOI: https://doi.org/10.1016/j.bios.2018.07.049
Reference: BIOS10638

To appear in: *Biosensors and Bioelectronic*

Received date: 21 May 2018
Revised date: 24 July 2018
Accepted date: 25 July 2018

Cite this article as: Bekir Çakıroğlu and Mahmut Özacar, A Self-Powered Photoelectrochemical Glucose Biosensor Based on Supercapacitor Co_3O_4-CNT Hybrid on TiO_2, *Biosensors and Bioelectronic,* https://doi.org/10.1016/j.bios.2018.07.049

A Self-Powered Photoelectrochemical Glucose Biosensor Based on Supercapacitor Co_3O_4-CNT Hybrid on TiO_2

Bekir Çakıroğlu[a], *Mahmut Özacar*[a, b*]

[a]*Sakarya University, Biomedical, Magnetic and Semiconductor Materials Research Center (BIMAS-RC), 54187 Sakarya, Turkey*

[b]*Sakarya University, Science & Arts Faculty, Department of Chemistry, 54187 Sakarya, Turkey*

*Corresponding Author. Tel.:+90 264 295 60 41; Fax:+90 264 295 59 50. *E-mail address:* mozacar@hotmail.com(M.Ozacar).

Abstract

In this study, a photoelectrochemical (PEC) biosensor was constructed by depositing supercapacitor carbon nanotubes (CNT) and Co_3O_4 onto the anatase TiO_2 coated ITO electrodes. Herein, supercapacitor Co_3O_4 was employed as a semiconductor with a band gap of ~2.07 eV, and the supercapacitor behavior of the PEC system was improved by introducing CNT into the electrode material. Furthermore, a self-empowering glucose biosensor operating at 0 volt was constructed for the first time. Also, upon the formation of p-n junction, Co_3O_4 was rendered electron accepting material, unlike its usual use in photocatalytic systems. Co_3O_4-CNT-anatase TiO_2 semiconductor hybrid was used to reduce recombination of exited electrons, and increasing the visible light absorption. Prior to enzyme immobilization, CNT containing electrode material was modified with 1-pyrene boronic acid via π-π interactions. The enzyme immobilization was carried out through covalent esterification between the boronic acid moiety and the carbohydrate part of GOx. Enzyme immobilization way enabled the close contact between FAD and electrode material, and the electron donor $FADH_2$ forming after the enzymatic reaction can give electrons to the photogenerated holes of Co_3O_4

through CNT along with H_2O_2 by enhancing the photocurrent. The obtained PEC biosensor demonstrated acceptable reproducibility and decent stability with a linear measurement range of 0 – 4 mM, a sensitivity of 0.3 $\mu AmM^{-1}cm^{-2}$, and lower detection limit of 0.16 µM. Thus, a self-powered biosensor was constructed by combining the PEC, and supercapacitor behavior of Co_3O_4 for the first time, and the utilization of the present PEC material can be extended to the other analytes detection through photoelectrochemistry. The supercapacitor materials led to the high current at direct electron transfer potential range, and this phenomenon implies that the PEC electrode can also be used in biofuel cells to obtain high power.

Keywords: Co_3O_4; Carbon nanotube; Supercapacitor; Glucose oxidase; Photoelectrochemical biosensor.

1. Introduction

The photoelectrochemical (PEC) bioanalysis has been emerged as a state-of-the-art analytical technique for the determination of biologically, and environmentally important analytes due to the simplicity, fast response, low-cost determination, low background and, high sensitivity (Zhao et al., 2015). The PEC biosensors can even operate without external voltage, avoiding inherent poor anti-interference capability of the PEC biosensors. This type of "self-powered" PEC biosensors operates at 0 V, and is a hot topic in the biosensor area (Zhao et al., 2016; Kang et al., 2016; Dai et al., 2017). The utilization of compatible semiconductors, which have appropriate band alignment in PEC system is of great importance for the efficient photocurrent generation. The coupling of small band gap semiconductors with the large band gap ones enhances the charge separation by suppressing the electron-hole recombination, which results in amplification of photocurrent generation (Zang et al., 2017). Titanium dioxide (TiO_2) with a wide band gap (3.20 eV) is one of the most used n-type semiconductors owing to its good biocompatibility, high electronic mobility, and chemical stability, facile

surface modification and can be obtained in an easy and low-cost way (Huo et al., 2015). However, the large band gap of TiO_2 leads to the excitation mainly under UV irradiation with substantial recombination. To overcome this problem, the visible light activity of TiO_2 has been enhanced by metal, nonmetal doping, coupling with a narrow band gap semiconductors, and metal nanoparticles, and dye binding on the TiO_2 surface (Liu et al., 2015; Fan et al., 2016; Çakar and Özacar, 2017). Cobalt oxide (Co_3O_4) possesses a versatile use due to the fact that Co_3O_4 is a p-type semiconductor with a band gap of ~2.07 eV, and excellent candidate for supercapacitor electrode material owing to its high theoretical capacitance (3560 $F.g^{-1}$) (Wang et al., 2009). Considering conductance band (CB) and valance band (VB) position, Co_3O_4 has been widely used for the photocathode fabrication in water splitting, and CO_2 reduction studies. In these studies, the electrons in the CB of Co_3O_4 are scavenged by electron acceptor species, such as H^+, and CO_2 (Xie et al., 2016). However, upon the formation of p-n junction, the VB of Co_3O_4 can be scavenged by electron donor species, and can be employed in photoanode construction (Tang et al., 2014b). One-dimensional nanostructures, such as nanowires and nanotubes, can lead to the fast charge transport through the micrometer-scale axial lengths, along with the efficient charge separation across the nanometer-scale diameters. In this context, single-walled carbon nanotubes (CNT) as a conducting scaffold material in a TiO_2 based PEC devices leads to the increase in the photoconversion efficiency. The length of the CNTs is of great importance for the improved photocurrent generation and probably the defects in the CNT affect the extent of charge separation (Sheeney-Haj-Ichia et al., 2004). Carbon nanotubes (CNT) have been widely used in PEC systems owing to their unique one-dimensional nanostructure and appropriate band energy (Kilic et al., 2016). Recently, enzyme based photoelectrodes have been constructed for the detection of important analytes by combining sensitivity of PEC system and selective of enzymes (Zhu et al., 2016). Although, there is one study reporting Co_3O_4-TiO_2 composite (Huang et al., 2015), there is need for the

cheaper and more facile Co_3O_4-TiO_2 composite synthesis by improving conductivity, and enzyme immobilization with the addition of CNT, and contributing the explanation of the effect of p-n junction formation for the biosensor systems.

Herein, a new visible light sensitive TiO_2-CNT-Co_3O_4 hybrid semiconductor was used for the construction of self-powered glucose biosensor. A PEC biosensor was formed with the formation of p-n junction between TiO_2 and Co_3O_4 nanoparticles (NPs), which leads efficient photocurrent generation. The specificity of the GOx was combined with the sensitivity of the PEC analysis. In addition, the as-prepared TiO_2-CNT-Co_3O_4 heterojunctions has a broad absorption spectrum in the visible region, and have satisfying photoelectrochemical performance, which results from the decent electron transitions and carrier effective separations compared to single TiO_2 and TiO_2-Co_3O_4.

2. Experimental Section

2.1. Apparatus and reagents

Glucose oxidase (GOx) (E.C.1.1.3.4., Type II, 17300 U g^{-1}) from *Aspergillus niger*, Indium tin oxide coated glass slide electrodes (ITO), titanium (IV) isopropoxide (TIP) (97%), 1-pyrene boronic acid, single-walled carbo nanotubes (SWNT), ethanol (anhydrous, ≥99.8%), ammonium hydroxide (25-30% HH_3 basis), D-(+)-maltose monohydrate, dopamine hydrochloride, uric acid and methanol were purchased from Sigma-Aldrich. D (+) glucose monohydrate, ascorbic acid and Cobalt (II) acetate tetrahydrate were obtained from Merck, and a stock solution of 1 M glucose was prepared and allowed to mutarotation overnight prior to use. Phosphate buffer solution (PBS) was prepared by using NaH_2PO_4, Na_2HPO_4 (Sigma-

Aldrich). All chemicals were used as received and without further purification. Deionized water (DW) was obtained from Labconco Water Pro BT purification system.

2.2. Preparation of TiO_2 NPs

In a typical experiment, 5 mL ammonium hydroxide was poured into 20 mL ethanol under vigorous stirring. Then, 200 µL of TIP was added into the mixture, and the solution was kept under stirring for 2 h. The obtained particles were centrifuged out at 11000 rpm for 20 min and then re-suspended in DW. Finally, the product was dried in oven at 60 °C overnight.

2.3. Synthesis of Co_3O_4 NPs

0.50 g of Cobalt (II) acetate tetrahydrate was dissolved in a solution consisting 10 mL DW, and 15 mL ethanol, and 2.5 mL of ammonium hydroxide was added under vigorous stirring. The mixture was stirred for 10 min to form a homogeneous suspension. Then the suspension was transferred into a 48.0 mL autoclave, sealed and maintained at 150 °C for 3 h. After cooling to room temperature, the black product was washed with DW prior to centrifugation, and was re-dispersed again in DW, dried at 60 °C for 4 h.

2.4. Fabrication of PEC electrodes

The PEC biosensor was fabricated on an ITO electrode (L × W × thickness, 75 mm × 25 mm × 1.1 mm and surface resistivity 8-12 Ω/sq). Briefly, the ITO electrodes were pre-cleaned by sonication in acetone, sodium hydroxide solution (1 M) in ethanol/water mixture (1:1, v/v),

and water for 15 min, and then dried in a vacuum oven prior to nanocomposite coating. Then, 8 µL TiO_2 suspensions with a concentration range of 3-15 mg mL^{-1} were drop-casted on to the ITO electrodes, and the electrodes were sintered at 450 °C for 30 min to form an anatase TiO_2 film (ITO/TiO_2). Then, 8 µL of Co_3O_4-CNT suspensions with the ratio range from 1:3 to 3:3 were drop-casted on ITO/TiO_2 electrode (ITO/TiO_2-Co_3O_4-CNT). After completely drying in air, the electrodes were kept in 10 mM 1-pyrene boronic acid in methanol for 2 h, and then incubated in 10 mg mL^{-1} GOx in 0.1 M PBS (pH=7.4) for 4 h at 4 °C, and the prepared electrodes (ITO/TiO_2- Co_3O_4-CNT-GOx) were used as PEC biosensor in the experiments.

2.5. Characterization of Photoelectrochemical Materials

PEC measurements were performed on CHI 660C electrochemical workstation equipped with a 400 W halogen lamp (Pelsan, wavelength range: 400-700 nm) as irradiation source for the photocurrent measurements. The modified ITO electrode with a material coated area of 0.0475 cm^2, a Pt wire and a saturated Ag/AgCl was employed as the working, counter and reference electrode, respectively. The photocurrent measurements were performed at a constant potential of 0 V (vs saturated Ag/AgCl) in 0.1 M PBS. Electrochemical impedance spectroscopy (EIS) study was performed on a CHI 660C electrochemical workstation (CH Instruments, Austin, TX, USA) in a 0.1 M KCl solution containing 5.0 mM $K_3[Fe(CN)_6]/K_4[Fe(CN)_6]$ (1:1) at open circuit voltage with an amplitude of 5 mV over a frequency range of 0.01 Hz-10 kHz. The transmission electron microscopy (TEM) studies were carried out with a FEI TALOS F200S operating at a voltage of 200 keV. The X-ray diffraction (XRD) analyses were performed by using an X-ray diffractometer (PANalytical–

Empyrean), with CuKα radiation. UV-Visible (UV–Vis) absorption spectroscopic measurements were carried out using a Shimadzu UV-2600 spectrophotometer (Shimadzu, Japan).

3. Results and Discussion

3.1. The construction of the PEC device

The fabrication of PEC system was illustrated in Scheme 1A. TiO_2 NPs were synthesized by using facile sol-gel procedure. Upon the sintering at 450 °C, anatase film was obtained on the ITO surface. After the deposition of Co_3O_4 and CNT on the film, p-n heterojunction occurs between p type Co_3O_4 NPs and n type TiO_2 NPs. Prior to the GOx immobilization, CNT on the surface of electrode were modified with pyrene bearing boronic acid moiety via π-π interactions. GOx was immobilized through the esterification of boronic acid–diol moieties of the carbohydrate part of GOx (Reuillard et al., 2014). When considering the content of carbohydrate as 16 %, this immobilization can be very favorable. The TiO_2 coating on ITO electrode was optimized, and the maximum photocurrent was obtained on the concentration of 9 mg mL^{-1} (Fig. S1.A). Also, optimum volume Co_3O_4:CNT ratio was found to be 3:3, and this ratio was used during biosensor fabrication (Fig. S1.B).

Scheme 1 position

The TEM images of materials were demonstrated in Fig. 1. The aggregates were observed in TiO_2 sample with a nanoparticle diameter of 17 nm, and the lattice spacing of 0.35 nm, which

corresponds to the *d*-spacing of (101) plane of anatase structure (Fig. 1.A, B). Co_3O_4 NPs were found to be strongly attached to CNT in the images with a diameter of ca. 6 nm and the lattice spacings of 0.25 nm, and 0.28 nm, which correspond to the *d*-spacings of (311) (220) planes of crystalline Co_3O_4 (Fig. 1.C, D, E). In Fig.1.F, TiO_2 NPs adjoin Co_3O_4 NPs, which can demonstrate the possible p-n junction formation. Energy dispersive X-ray spectroscopy analysis confirmed the presence of elements, which form the intact nanocomposite, with an appropriate ratio (Fig. S2).

Figure 1 position

As for the XRD patterns, Fig. 2A (a) confirms the formation of pure anatase phase of TiO_2 (ICDS: 98-015-4601). The peaks of Co_3O_4 demonstrate the cubic spinel-type structure at 2θ values of 18.90°, 31.29°, 36.81°, 44.80°, 59.37° and 65.27° corresponding to (111), (220), (311), (400), (511) and (440) crystalline planes of Co_3O_4 (ICDS: 04-003-0984) (Fig. 2A (b). In Fig. 2A (c) demonstrated a pattern, which displays all of the materials in the intact electrode. The peaks related to ITO with the crystalline planes of (222), (400), (440), and (622), and the peak associated to CNT with the crystalline plane of (100) were observed along with the peaks related to TiO_2 and Co_3O_4. UV-Vis spectrum of Co_3O_4 NPs was demonstrated in Fig. 2B. The intense band appeared at 410 nm is attributed to the $O^{2-} \rightarrow Co^{2+}$ charge transfer with the electronic band gap energy of 2.07 eV, and the slight absorption band at 690 nm can be assigned to $O^{2-} \rightarrow Co^{3+}$ charge transfer with the electronic band gap energy of 1.45 eV (Zhang et al., 2013). This spectrum confirms the strong visible light absorption of Co_3O_4 NPs.

Figure 2 position

Cyclic voltammetry (CV) measurements of GOx immobilized electrodes were carried out in 0.1 M PBS (pH 7.4). In Fig. 2C, a pair of redox peaks were observed in deoxygenated PBS with the anodic peak potential at -390 mV and the cathodic peak potential at -510 mV. The formal potential calculated from the average of cathodic and anodic peak potential is -450 mV. This value is close to the standard electrode potential of FAD/$FADH_2$ (vs. Ag/AgCl), confirming that GOx was closely immobilized on the nanocomposite material (Çakıroğlu and Özacar, 2017). The reduction current was increased in oxygenated PBS containing 20 mM glucose. This reduction current is the required value to reduce the remaining oxidized form FAD from the glucose oxidation. However, under the visible light illumination, the reduction current even more increased, confirming the intense effect of PEC material on the efficient electron transfer. Also, the large faradaic current value with high electrostatic double layer capacitance, which is deduced from the large area of CV graphs, demonstrated the supercapacitor behavior of the hybrid material (Pankratov et al., 2014; Veeramani et al., 2016).

The potential yielding the maximum current was determined by linear sweep voltammetry (LSV) for the next glucose measurement studies. Fig. 2D demonstrates the LSV curves of the electrodes in oxygenated PBS containing 20 mM glucose under visible light. No reduction-oxidation reaction was observed by using the ITO, and ITO/TiO_2 electrodes (Fig. 2D (a), and (b)), demonstrating little to no activity of the electrode material. However, upon the deposition of CNT on the ITO/TiO_2 electrode, a substantially increased current centered at about 0 V was observed owing to the fact that CNT can be excited under the visible light, and

at an appropriate potential, a photocurrent can be observed with the direct glucose oxidation (Fig. 2D (c)) (Liu et al., 2012; W. Liu et al., 2017a). The addition of Co_3O_4 led to the more improved current at 0 V owing to the reinforcement of semiconductor behavior of the electrode material (Fig. 2D (d)). Co_3O_4 NPs can be excited under the visible light irradiation (Tang et al., 2014b). The most enhanced photocurrent generation was achieved by using the ITO/TiO_2-Co_3O_4-CNT-GOx electrode owing to the releasing H_2O_2, which acts as electron donor for the photogenerated holes along with $FADH_2$ (Fig. 2D (e)) (Wu et al., 2017).

3.2. Photocurrent generation of ITO/TiO_2-CNT-Co_3O_4-GOx PEC electrode

Hybrid materials containing connected n-type semiconductor and p-type semiconductor lead to one direction electron transfer from p-type to n-type semiconductor upon the formation of depletion region via diffusion current. In the constructed hybrid, electrons flow from p-type semiconductor Co_3O_4 to n-type semiconductor TiO_2 intrinsically (Lang et al., 2016). The n-type semiconductor behavior of TiO_2 originates from oxygen vacancies and p-type semiconductor behavior of Co_3O_4 is associated to the cation vacancies. Upon visible light irradiation, the electron–hole pairs are generated on Co_3O_4, and then the photogenerated electrons are rapidly injected from the CB of Co_3O_4 to the CB of TiO_2. The simultaneous charge separation is thermodynamically favorable as the potential of the CB of Co_3O_4 is higher than that of TiO_2. Finally, the electrons transfer to ITO, while the photogenerated holes in the VB of TiO_2 migrate to the VB of Co_3O_4. H_2O_2, releasing from the enzymatic reaction, can be utilized as an electron donor for efficient scavenging of photogenerated holes on

Co_3O_4 NPs (Tang et al., 2014a; P. Liu et al., 2017b). Also, the hole scavenging was enhanced with the close attachment of $FADH_2$, which is formed upon the enzymatic glucose oxidation. This phenomenon has a synergistic effect on the photocurrent generation, and CNT can hasten the charge separation, and retard the electron-hole recombination along with the excellent electron transfer. Also, semiconducting CNT possess a band gap suitable to visible-light wavelengths, and an additional excitation in the material can increase the photocurrent. On the basis of the above ideas, the glucose measurements were carried out by using fabricated PEC biosensor (Scheme 1B).

3.3. Photocurrent response of the electrodes and PEC glucose sensing

Photocurrent measurements were carried out by exposing the PEC electrodes to 5 mM glucose solution. As can be seen from Fig. 3A (a), a slight photocurrent was observed for the bare ITO electrode under the light irradiation. ITO/TiO_2 electrode exhibited a photocurrent of 100 nA resulted from the poor visible light absorbance of TiO_2 (Fig. 3A (b)). Upon the deposition of Co_3O_4 NPs on the ITO/TiO_2 electrode, the photocurrent response increased to some extent owing to the visible light absorption and charge transfer on the excited Co_3O_4 NPs owing to the p-n junction formation (Fig. 3A (c)). ITO/TiO_2-Co_3O_4-CNT electrode gave a more improved photocurrent (Fig. 3A (d)). Herein, CNT leads to photocurrent enhancement by reducing the charge recombination along with improving electrical conductivity (Shastry and Hersam, 2017). Finally, enzyme electrode demonstrated the most enhanced photocurrent owing to the scavenging of photogenerated holes by releasing product H_2O_2 along with $FADH_2$ (Fig. 3A (e)). Enzyme immobilization method enabled the direct electron transfer

between FAD and electrode material, and the close contact improved the photocurrent owing to the fact that the electron donor $FADH_2$ forming after the enzymatic reaction can give electrons to the photogenerated holes of Co_3O_4 through CNT. Only GOx immobilized electrode yielded a specific response to glucose solution. The optimum buffer solution pH and operation potential were found to be pH 7.4, and 0 V, respectively as demonstrated in Fig. S3 A, and B. Owing to the denaturation of protein structure, photocurrent diminished towards strong acidic and basic medium. At positive voltages, photocurrent increased owing to H_2O_2 oxidation. However, negative direct electron transfer potential affected the optimum photocurrent voltage by shifting the positive potential for H_2O_2 oxidation to 0 V. At negative voltages, photocurrent diminished owing to the suppressed H_2O_2 oxidation. Also, EIS studies elucidated the conductivity change upon step-wise material deposition (Fig. S4).

Figure 3 position

The time-dependent PEC photocurrent (i–t) measurements were taken in oxygenated 0.1 M PBS (pH 7.4) containing different glucose concentrations at 0 V by using the enzyme immobilized electrode. GOx can catalyze the electro-oxidation of glucose by producing H_2O_2. Herein, the visible light illumination leads to the generated holes on Co_3O_4 NPs, and the holes can be scavenged by generating photocurrent in proportion to H_2O_2 and $FADH_2$, which is produced during enzymatic glucose oxidation. The glucose measurement results were displayed in Fig. 3B. The photocurrent increased directly proportional to the glucose concentration at a certain range, and then reached a plateau, which demonstrates Michaelis-Menten kinetics (Fig. 3C). In Fig. 3D, the linear part of the graph demonstrated a regression equation as photocurrent (nA) = $13.9C_{glucose}$ (mM) + 135.84 (R^2 = 0.996). The linear measurement range was found to be in the range of 0 – 4 mM glucose, with a sensitivity of 0.3 $\mu AmM^{-1}cm^{-2}$. The limit of detection

(LOD) was calculated by using the formula, LOD = 3 S_b/S (S_b: standard deviation of ten blank measurements and S: sensitivity), and was found to be 0.16 µM. The current study was compared to some of the self-powered enzyme based biosensors in Table 1.

Although self-powered biosensors are based on biofuel cell type systems, and biocapacitor based systems in the literature (Hickey et al., 2016; Sode et al., 2016), PEC biosensors yielding response at 0 V can be an alternative to the other self-powered biosensors owing to facile sensing with an uncomplicated system. Owing to the scarce articles on self-powered glucose biosensor, we have compered the present study to the all kinds of biosensors reported in the literature. The satisfactory linear range of the biosensor can be attributed to the hybrid nature of the electrode nanomaterial. According to the Table 1, the biosensors composed of one semiconducting material demonstrated narrow linear measurement range due to the poor electrical conductivity, and insufficient photocurrent generation. The combination of other semiconducting materials with TiO_2 can enlarge the measurement range owing to the enhanced photocurrent generation. However, PEC based biosensors require a positive potential for the scavenging of photogenerated holes by H_2O_2. In this study, owing to the close contact of $FADH_2$ with the semiconductor material, $FADH_2$ can also scavenge the holes. Owing to the negative potential of $FADH_2$ oxidation, a synergistic effect can be observed on the photocurrent generation by shifting the optimum photocurrent potential to 0 V.

3.4. Repeatability, reproducibility and stability of the self-powered biosensor

The stability, repeatability, and reproducibility of the PEC biosensor were determined in 5 mM glucose containing PBS. Upon the repeated on–off visible light illumination, the photocurrent remained nearly constant with the relative standard deviation (RSD) of 1.1% (Fig. 4A). The five electrodes prepared independently under the same conditions were demonstrated decent reproducibility with an RSD of 5.7% (Fig. S5). The photocurrent response maintained 90.8% of its initial response after the storage at 4 °C for 6 weeks (Fig. S6). The decent stability, and repeatability results from the robust immobilization of enzyme (Çakıroğlu et al., 2018), and satisfying reproducibility is attributed to the facile and sturdy construction.

3.5. Interfering effect and glucose determination in real samples

Ascorbic acid (AA) and uric acid (UA), and dopamine (D) are easily oxidized, and they can coexist with glucose in the biological fluids. The addition of 0.2 mM AA, UA, D and maltose (MA) to the 1 mM glucose solution led to no observable photocurrent change (Fig. 4B). The change of the photocurrent corresponded to an RSD of 6.1% upon the addition of all interfering substances, confirming GOx selectivity. Also, oxidation of the substances was ruled out at low operating voltage, *viz*. 0 V.

The practical application of the PEC biosensor was carried out to detect glucose in human serum samples with 2 times dilution of sample. The human serum sample was also analyzed with photometric kits. The recovery tests were carried out by adding 0.3 mM glucose solution aliquots to the serum solution. The glucose concentration was found to be 4.8 mM with a

recovery value of 91.6%. The RSD value meets the satisfying accuracy for analysis in real samples.

3.6. Electrochemical glucose determination

Owing to reaching high current values, electrochemical biosensor studies were also carried out to obtain larger sensitivity. The PEC electrode demonstrated enzymatic glucose oxidation. Fig. 4C and Fig. S7 display the choronoamperometric curves of glucose measurements with or without light illumination, respectively. The cathodic currents decreased linearly with the increase of glucose concentration in O_2-saturated PBS.

$$\mathrm{GOD\ (FAD)} + \mathrm{glucose} \rightarrow \mathrm{gluconolactone} + \mathrm{GOD\ (FADH_2)} \quad (1)$$

According to the electrochemical reaction (equation 1), the reduced form of FAD ($FADH_2$) increases upon the glucose oxidation. Therefore, reduction current for the FAD decreases with the increasing glucose concentration (Akkaya et al., 2018). The calibration curves are linear in the glucose concentration range of 0-7 mM, after which the reduction current reached a plateau (Fig. 4D). The plots displayed a typical Michaelis–Menten enzyme kinetics. The sensitivity of the biosensor was found to be 33.33 $\mu AmM^{-1}cm^{-2}$ with a R^2 of 0.9984 without light illumination. However, upon the visible light illumination, the sensitivity even more increased to 44.88 $\mu AmM^{-1}cm^{-2}$ with a R^2 of 0.9982 with an LOD of 0.20 µM. This improvement of sensitivity under light illumination can be attributed to the semiconducting behavior of nanocomposite. When compared to the self-powered PEC response, more

improved sensitivity was observed by carrying out electrochemical measurements owing to taking advantage of semiconductor, and supercapacitor behavior of electrode material.

4. Conclusions

In summary, a hybrid composite with the p-n junction semiconductor system was successfully obtained for the PEC biosensor fabrication. Owing to the supercapacitor behavior of CNT and Co_3O_4 NPs, high current value was observed, which can be beneficial electrochemical systems. The formation of p-n junction between TiO_2 NPs and Co_3O_4 NPs was confirmed according to the photocurrent increment owing to the enhanced separation of the photogenerated electron-hole pairs. The fabricated biosensor can be used in PEC, and electrochemical mode owing to the conductive, supercapacitive, and semiconducting nature of the fabricated hybrid material. The PEC biosensor yielded a linear response to 0-4 mM glucose concentration at 0 V. Therefore, a self-powered biosensor was constructed by combining the PEC, and supercapacitor behavior of Co_3O_4 for the first time, and the utilization of PEC material can be extended to the detection of other analytes based on photoelectrochemistry. The introduction of other semiconductors, and metal nanoparticles can even more improve the biosensor performance, but at the expense of cost. High current values according to CV curves imply that the electrode can also be used in biofuel cells to obtain high power.

Acknowledgements

This study was supported by the Scientific Research Projects Commission of Sakarya University (Project number: 2017-02-04-024, 2017-02-04-050, and 2017-50-01-078). M.O. thanks Turkish Academy of Sciences (TUBA) for partial support.

References

Akkaya, B., C□akıroğlu, B., Özacar, M., 2018. ACS Sustain. Chem. Eng. 6, 3805–3814.

Bao, S.J., Li, C.M., Zang, J.F., Cui, X.Q., Qiao, Y., Guo, J., 2008. Adv. Funct. Mater. 18, 591–599.

Çakar, S., Özacar, M., 2017. J. Photochem. Photobiol. A Chem. 346, 512–522.

Çakıroğlu, B., Çiğil-Beyler, A., Ogan, A., Kahraman, M.V., Demir, S., 2018. Eng. Life Sci 18, 254–262.

Çakıroğlu, B., Özacar, M., 2017. Electroanalysis 29, 2719 –2726.

Dai, W.X., Zhang, L., Zhao, W.W., Yu, X.D., Xu, J.J., Chen, H.Y., 2017. Anal. Chem. 89, 8070−8078.

Fan, G.C., Zhao, M., Zhu, H., Shi, J.J., Zhang, J.R., Zhu, J.J., 2016. J. Phys. Chem. C 120, 15657–15665.

Fischer, C., Fraiwan, A., Choi, S., 2016. Biosens. Bioelectron. 79, 193–197.

Hickey, D.P., Reid, R.C., Milton, R.D., Minteer, S.D., 2016. Biosens. Bioelectron. 77, 26–31.

Huang, B., Yang, W., Wen, Y., Shan, B., Chen, R., 2015. ACS Appl. Mater. Interfaces 7, 422–431.

Huo, H., Xu, Z., Zhang, T., Xu, C., 2015. J. Mater. Chem. A 3, 5882–5888.

Kang, Z., Yan, X., Wang, Y., Zhao, Y., Bai, Z., Liu, Y., Zhao, K., Cao, S., Zhang, Y., 2016. Nano Res. 9, 344–352.

Kilic, B., Turkdogan, S., Astam, A., Ozer, O.C., Asgin, M., Cebeci, H., Urk, D., Mucur, S.P.,

2016. Sci. Rep. 6, 1–9.

Lang, D., Cheng, F., Xiang, Q., 2016. Catal. Sci. Technol. 6, 6207–6216.

Liu, W., Wu, X., Li, X., 2017a. RSC Adv. 7, 36744–36749.

Liu, P., Huo, X., Tang, Y., Xu, J., Liu, X., Wong, D.K.Y., 2017b. Anal. Chim. Acta 984, 86–95.

Liu, X., Huo, X., Liu, P., Tang, Y., Xu, J., Liu, X., Zhou, Y., 2017c. Electrochim. Acta 242, 327–336.

Liu, X., Yan, R., Zhu, J., Xiaohe Huo, Wang, X., 2015. Electrochim. Acta 173, 260–267.

Liu, Y., Wang, D.P., Yu, Y.X., Zhang, W. De, 2012. Int. J. Hydrogen Energy 37, 9566–9575.

Min Ryu, G., Lee, M., Som Choi, D., Beum Park, C., 2015. J. Mater. Chem. B 3, 4483–4486.

Pankratov, D., Blum, Z., Shleev, S., 2014. ChemElectroChem 1, 1798 – 1807.

Reuillard, B., Le Goff, A., Holzinger, M., Cosnier, S., 2014. J. Mater. Chem. B 2, 2228–2232.

Selvarajan, S., Alluri, N.R., Chandrasekhar, A., Kim, S.J., 2016. Sensors Actuators, B Chem. 234, 395–403.

Shastry, T.A., Hersam, M.C., 2017. Adv. Energy Mater.

Sheeney-Haj-Ichia, L., Basnar, B., Willner, I., 2004. Angew. Chemie - Int. Ed. 44, 78–83.

Sode, K., Yamazaki, T., Lee, I., Hanashi, T., Tsugawa, W., 2016. Biosens. Bioelectron. 76, 20–28.

Tang, J., Wang, Y., Li, J., Da, P., Geng, J., Zheng, G., 2014a. J. Mater. Chem. A 2, 6153–6157.

Tang, J., Wang, Y., Wang, Y., Li, J., Kong, B., Jiang, M., Zheng, G., 2014b. J. Mater. Chem. A 2, 15752–15757.

Veeramani, V., Dinesh, B., Chen, S.-M., Saraswathi, R., 2016. J. Mater. Chem. A 4, 3304–3315.

Wang, G., Shen, X., Horvat, J., Wang, B., Liu, H., Guoxiu Wang, A., Wexler, D., Yao, J.,

2009. J. Phys. Chem. Part C Nanomater. Interfaces 113, 4357–4361.

Wu, S., Huang, H., Shang, M., Du, C., Wu, Y., Song, W., 2017. Biosens. Bioelectron. 92, 646–653.

Xie, S., Zhang, Q., Liu, G., Wang, Y., 2016. Chem. Commun. 52, 35–59.

Yan, Y., Fang, J., Yang, Z., Qiao, J., Wang, Z., Yu, Q., Sun, K., 2013. Chem. Commun. 49, 8632.

Zang, Y., Lei, J., Ju, H., 2017. Biosens. Bioelectron. 96, 8–16.

Zhang, L., Zhao, X., Ma, W., Wu, M., Qian, N., Lu, W., 2013. CrystEngComm 15, 1389–1396.

Zhao, K., Yan, X., Gu, Y., Kang, Z., Bai, Z., Cao, S., Liu, Y., Zhang, X., Zhang, Y., 2016. Small 2, 245–251.

Zhao, W.-W., Xu, J.-J., Chen, H.-Y., 2015. Chem. Soc. Rev. 44, 729–741.

Zhu, J., Huo, X., Liu, X., Ju, H., 2016. ACS Appl. Mater. Interfaces 8, 341–349.

Figure Captions

Scheme 1. A. PEC biosensor fabrication, and B. PEC biosensing mechanism for glucose.

Figure 1. A, and B. TEM images of TiO_2 NPs, C, and D. TEM images of Co_3O_4-CNT, E. TEM image of Co_3O_4, F. TEM image of Co_3O_4-TiO_2 NPs with the p-n junction.

Figure 2. A. XRD patterns of a. TiO_2, b. Co_3O_4, and c. intact electrode, B. UV-Vis spectrum of Co_3O_4. C. CV curves of a. ITO/TiO_2-CNT-Co_3O_4-GOx in deoxygenated PBS, b. oxygenated PBS with 20 mM glucose, and c. oxygenated PBS with 20 mM glucose under visible light. D. Linear sweep voltammograms of a. ITO, b. ITO/TiO_2, c. ITO/TiO_2-CNT, d. ITO/TiO_2-CNT-Co_3O_4, e. ITO/TiO_2-CNT-Co_3O_4-GOx.

Figure 3. A. Photocurrent generation for a. ITO, b. ITO/TiO_2, c. ITO/TiO_2-Co_3O_4, d. ITO/TiO_2-Co_3O_4-CNT, e. ITO/TiO_2-Co_3O_4-CNT-GOx, B. Glucose measurements in O_2 saturated PBS, C. Photocurrent responses vs. glucose concentration graph, D. The linear part of the responses vs. glucose concentration graph

Figure 4. A. Photocurrent stability of the fabricated PEC biosensor, B. Interfering effect of 0.2 mM AA, UA, D, and MA on photocurrent generation at 0 V, C. The chronoamperometric measurement of glucose by using PEC biosensor at -0.4 V under visible light, D. Current-concentration graph of biosensor under visible light (a), and without light illumination (b).

Table Captions

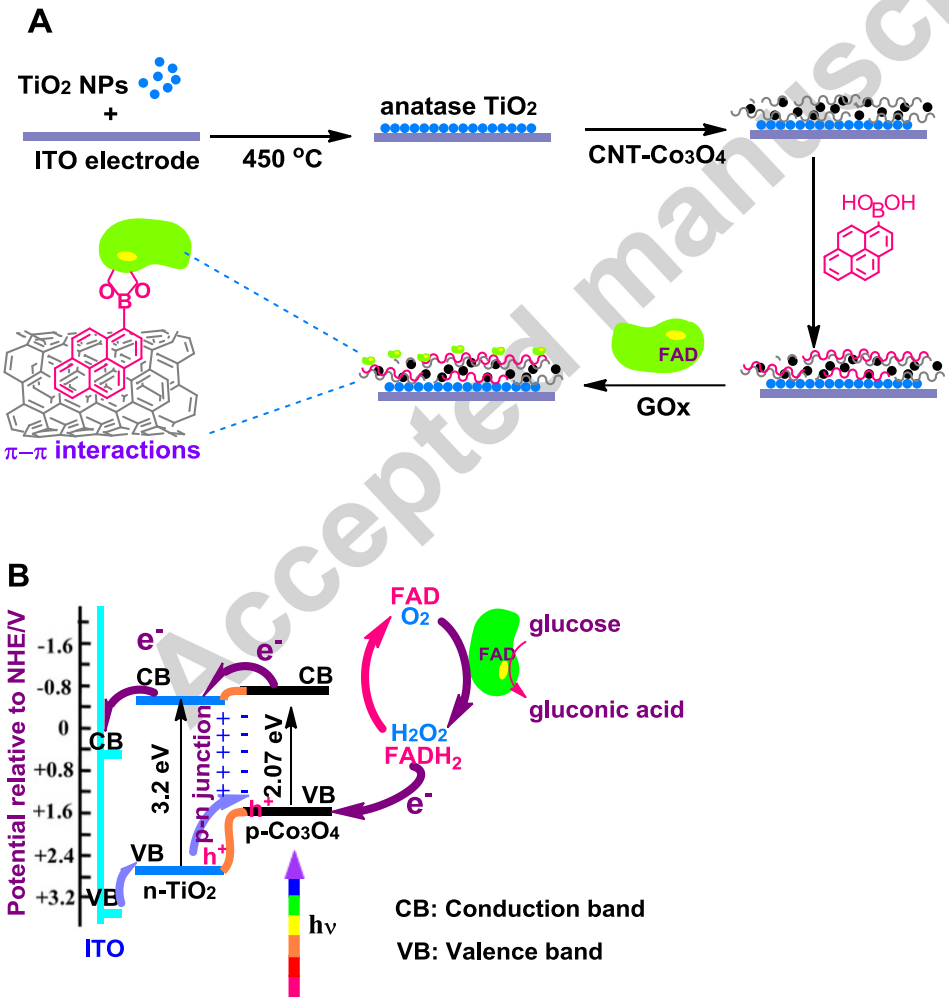

Scheme 1.

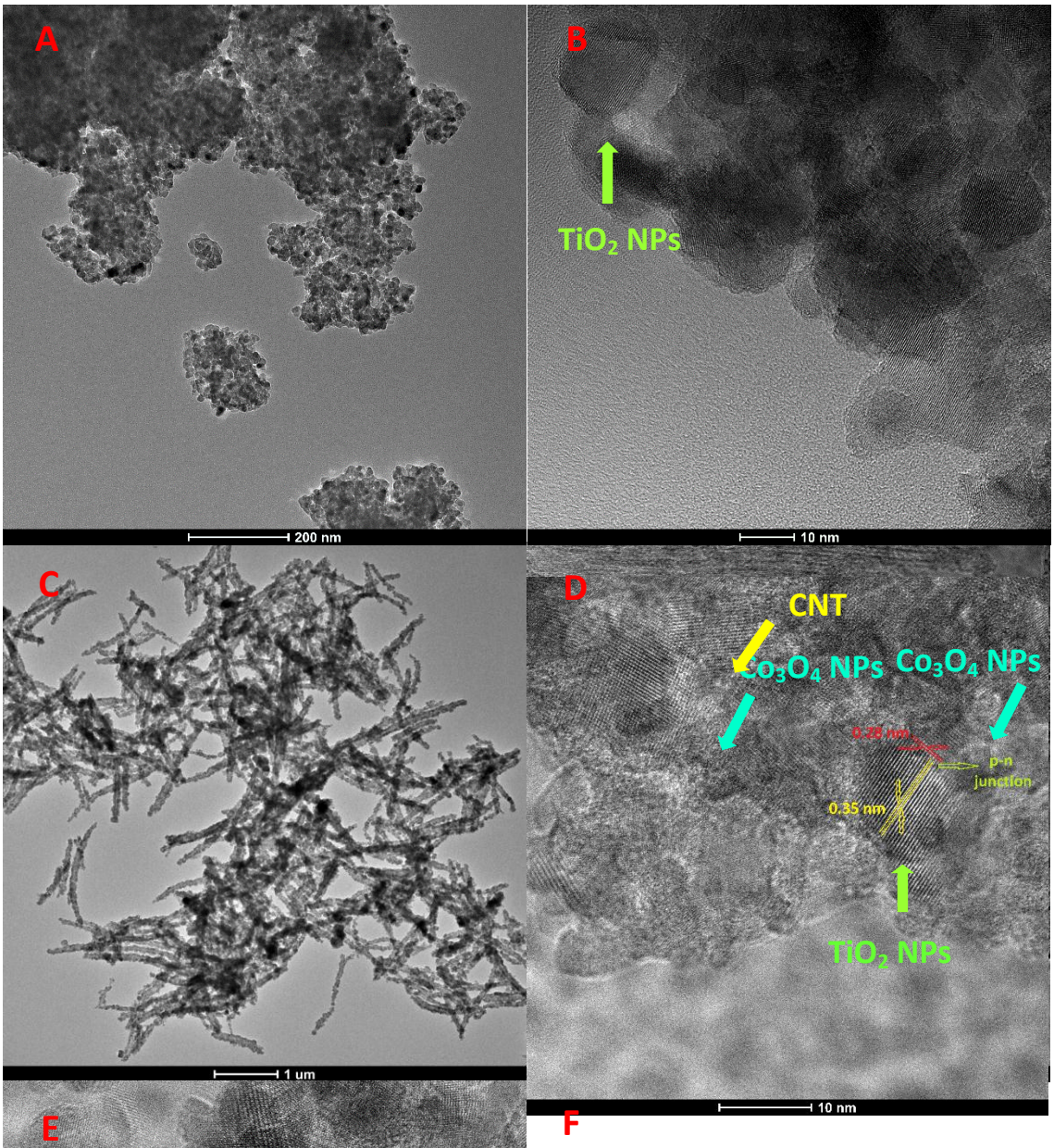
A
200 nm
B
TiO2 NPs
10 nm
C
1 um
D
CNT
Co3O4 NPs
Co3O4 NPs
0.26 nm
0.35 nm
p-n
junction
TiO2 NPs
10 nm
E
10 nm
F

Figure

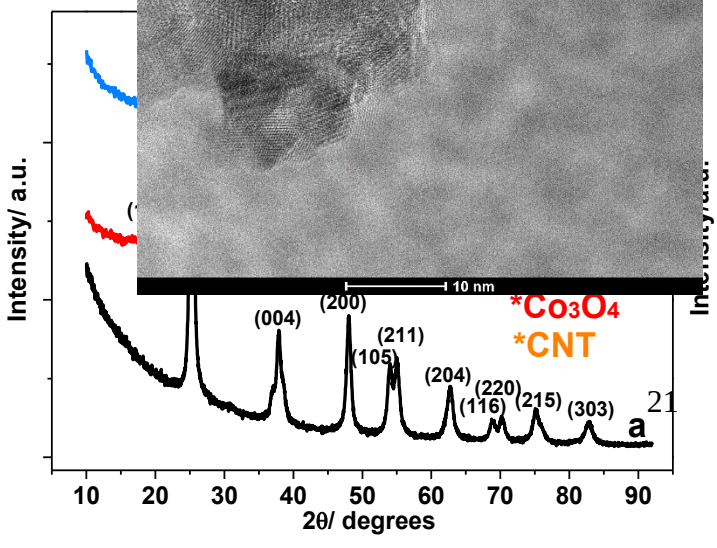
Intensity/ a.u.
(004)
(200)
(211)
(105)
(204)
(116)
(220)
(215)
(303)
*Co3O4
*CNT
a
10 20 30 40 50 60 70 80 90
2θ/ degrees

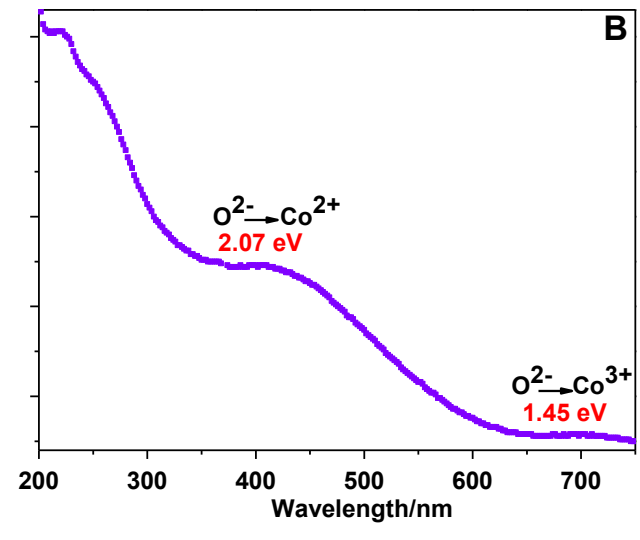
B
O2- → Co2+
2.07 eV
O2- → Co3+
1.45 eV
200 300 400 500 600 700
Wavelength/nm

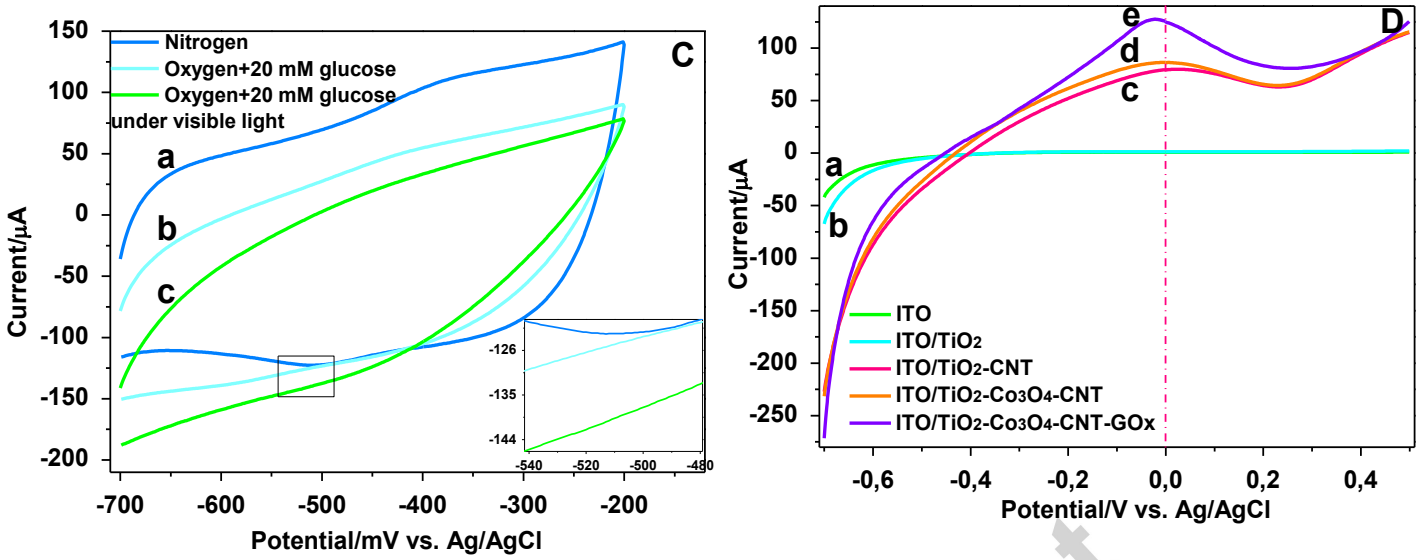

Figure 2.

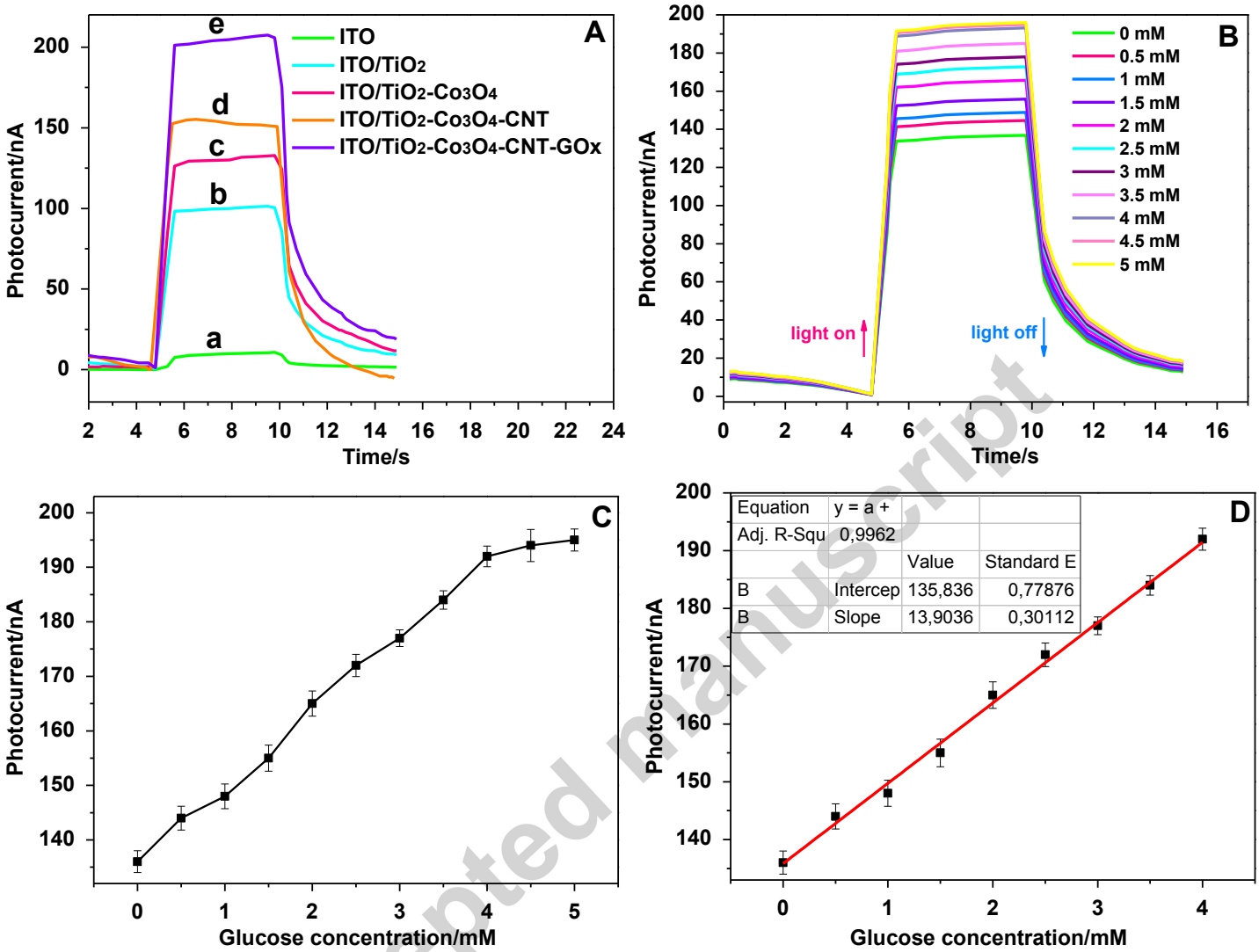

Figure 3.

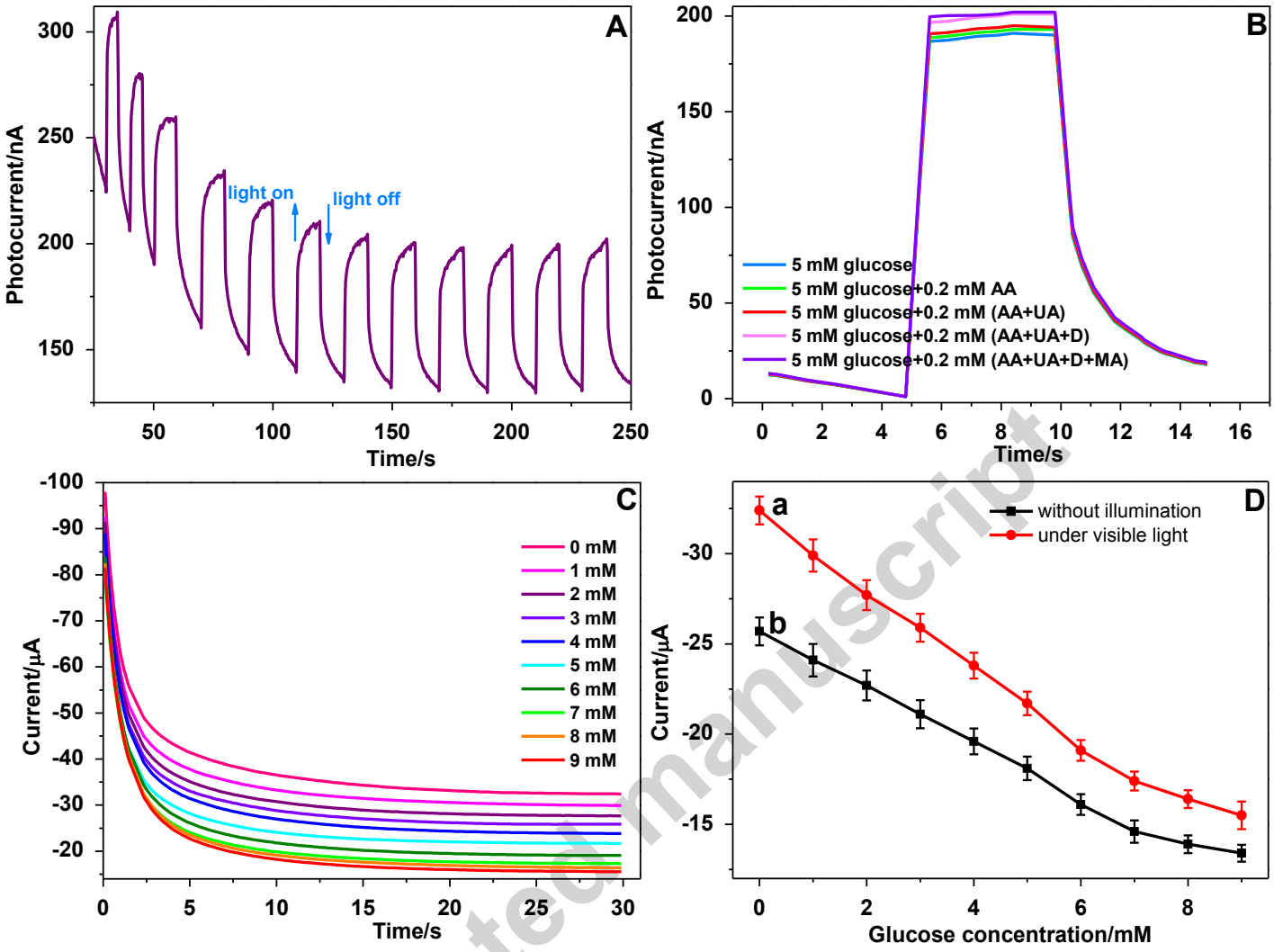

Figure 4.

Table 1. The comparison of analytical performances of PEC and electrochemical glucose biosensors

Biosensor composition	Operation potential/V vs. Ag/AgCl	LOD/μM	Linear range /mM	Sensitivity /$\mu AmM^{-1}cm^{-2}$	Ref.
ITO/TiO_2- Co_3O_4-CNT-GOx	0	0.16	0- 4	0.3	This study
Graphite/chitosan-GOx anode and carbon-based air cathode	OCVs[a]	-	1- 5	0.02	(Fischer et al., 2016)
TiO_2-GOx	-0.45	-	0.15- 1.2	0.3	(Bao et al., 2008)
FTO/ Fe_2O_3-NB-PDA-GDH[b]	0.05	25.2	0- 2	7.36	(Min Ryu et al., 2015)
ITO/TiO_2 (enzymeless)	0.4	-	0.02-5.0	-	(Yan et al., 2013)
Glass/$BaTiO_3$ (enzymeless)	0.5	7.941	0.0001–1	23.79	(Selvarajan et al., 2016)
ITO/TiO_2-MoS_2-GOx	0.2	15	0.1-10.5	0.81	(Liu et al., 2017)
ITO/MoS_2-GOx	0.6	0.00061	0.000008-0.005	-	(Wu et al., 2017)

[a] OCVs: Determination was carried out by observing the changes of open circuit voltages.

[b] NB-PDA-GDH: Nile Blue-polydopamine-glucose dehydrogenase

Highlights

- 0 V self-powered glucose biosensor was studied for the first time.
- Supercapacitor CNT-Co_3O_4 nanocomposite improved the current value.
- GOx based PEC biosensor with high sensitivity and selectivity was fabricated.
- Direct electron transfer was obtained for the efficient electron transmitting.
- $FADH_2$ oxidation had a synergistic effect on the H_2O_2 oxidation based photocurrent generation.